MRI atlas of the human hypothalamus.

Marc Baroncini, Patrice Jissendi, Eglantine Balland, Pierre Besson, Jean-Pierre Pruvo, Jean-Paul Francke, Didier Dewailly, Serge Blond, Vincent Prevot

Elsevier Editorial System(tm) for NeuroImage
Manuscript Draft

Manuscript Number: NIMG-10-486R3

Title: MRI atlas of the human hypothalamus

Article Type: Regular Article

Section/Category: Anatomy and Physiology

Corresponding Author: Dr Marc Baroncini, MD, PhD

Corresponding Author's Institution: Univ Lille Nord de France, F-59000 Lille, France

First Author: Marc Baroncini, MD, PhD

Order of Authors: Marc Baroncini, MD, PhD; Patrice Jissendi, MD, PhD; Eglantine Balland, PhD; Pierre Besson, PhD; Jean-Pierre Pruvo, MD, PhD; Jean-Paul Francke, MD, PhD; Didier Dewailly, MD, PhD; Serge Blond, MD, PhD; Vincent Prevot, PhD

Abstract: Gaining new insights into the anatomy of the human hypothalamus is crucial for the development of new treatment strategies involving functional stereotactic neurosurgery. Here, using anatomical comparisons between histology and magnetic resonance images of the human hypothalamus in the coronal plane, we show that discrete gray and white hypothalamic structures are consistently identifiable by MRI. Macroscopic and microscopic images were used to precisely annotate the MRI sequences realized in the coronal plane in twenty healthy volunteers. MRI was performed on a 1.5T scanner, using a protocol including T1-weighted 3D fast field echo, T1-weighted inversion-recovery, turbo spin echo and T2-weighted 2D fast field echo imaging. For each gray matter structure as well as for white matter bundles, the different MRI sequences were analyzed in comparison to each other. The anterior commissure and the fornix were often identifiable, while the mammillothalamic tract was more difficult to spot. Qualitative analyses showed that MRI could also highlight finer structures such as the paraventricular nucleus, the ventromedial nucleus of the hypothalamus and the infundibular (arcuate) nucleus, brain nuclei that play key roles in the regulation of food intake and energy homeostasis. The posterior hypothalamic area, a target for deep brain stimulation in the treatment of cluster headaches, was readily identified, as was the lateral hypothalamic area, which similar to the aforementioned hypothalamic nuclei, could be a putative target for deep brain stimulation in the treatment of obesity. Finally, each of the identified structures was mapped to Montreal Neurological Institute (MNI) space.

1. Cover Letter

juin 24, 2011

Dr Katrin Amunts

Section Editor,
Neuroimage

Dear Dr. Amunts,

Please find enclosed the revised version of our manuscript “MRI atlas of the human hypothalamus” which we have modified according to the minor comment made by the reviewer#3.

We appreciated the careful and incisive evaluation of our data made by the reviewers throughout the reviewing process. We hope that the manuscript is now in suitable form for publication in Neuroimage.

Sincerely,

Marc Baroncini, M.D., Ph.D.
Development and Plasticity of the Postnatal Brain
Jean-Pierre Aubert Research Center
Inserm U837/University of Lille 2
Bâtiment Biserte
1 place de Verdun
59045 Lille cedex
France

***4. Highlights**

- New insights into the anatomy of the human hypothalamus
- Specific 1.5T MRI sequences approach histological resolution within the hypothalamus
- White matter bundles within the hypothalamus can be identified using 1.5T MRI
- Hypothalamic gray structures can be identified using 1.5T MRI

***6. Response to Reviews**

We have revised our manuscript to address the minor point raised by reviewer 3.

In the “Data analysis” paragraph of the materials and methods section it now reads: “Structures were identified visually based on our knowledge of specific landmarks obtained from anatomical-histological cross sections and with reference to previously published atlases (Swaab et al., 1993; Koutcherov et al., 2000, 2004; Koutcherov et al., 2007; Mai et al., 2008); the landmarks used, such as the optic tract, the floor of the diencephalon, the third ventricle, and the fornix, were readily and reliably identifiable in MR scans.”

YNIMG NIMG-10-486R3 Revised: June 24, 2011
Neuroimage

MRI atlas of the human hypothalamus

Marc Baroncini [a, b, c, d *], Patrice Jissendi [b, e], Eglantine Balland [a, b], Pierre Besson [e], Jean-Pierre Pruvo [b, e], Jean-Paul Francke [a, b, c], Didier Dewailly [b, f], Serge Blond [a, b, d], Vincent Prevot [a, b, d]

[a] Inserm, Jean-Pierre Aubert Research Center, U837, Development and Plasticity of the postnatal Brain, Place de Verdun, F-59045 Lille cedex, France
[b] Univ Lille Nord de France, F-59000 Lille, France
[c] UDSL, Laboratory of Anatomy, Faculty of Medicine, Place de Verdun, F-59045 Lille cedex, France
[d] CHRU Lille, Department of Neurosurgery, Lille University Hospital, 59037 Lille cedex, France
[e] CHRU Lille, Department of Neuroradiology, Lille University Hospital, 59037 Lille cedex, France
[f] CHRU Lille, Department of Endocrine Gynecology and Reproductive Medicine, Lille University Hospital, 59037 Lille cedex, France

Number of text pages: 30
Number of figures: 7
Number of tables: 5
Number of words (abstract): 247
Number of words (introduction): 739
Number of words (discussion): 1638

*__Corresponding author:__ Marc Baroncini, M.D., Ph.D. – Inserm, Jean-Pierre Aubert Research Center, U837, Development and Plasticity of the postnatal Brain, Place de Verdun, F-59045 Lille cedex, France.
E-mail: marc.baroncini@inserm.fr

Abstract

Gaining new insights into the anatomy of the human hypothalamus is crucial for the development of new treatment strategies involving functional stereotactic neurosurgery. Here, using anatomical comparisons between histology and magnetic resonance images of the human hypothalamus in the coronal plane, we show that discrete gray and white hypothalamic structures are consistently identifiable by MRI. Macroscopic and microscopic images were used to precisely annotate the MRI sequences realized in the coronal plane in twenty healthy volunteers. MRI was performed on a 1.5T scanner, using a protocol including T1-weighted 3D fast field echo, T1-weighted inversion-recovery, turbo spin echo and T2-weighted 2D fast field echo imaging. For each gray matter structure as well as for white matter bundles, the different MRI sequences were analyzed in comparison to each other. The anterior commissure and the fornix were often identifiable, while the mammillothalamic tract was more difficult to spot. Qualitative analyses showed that MRI could also highlight finer structures such as the paraventricular nucleus, the ventromedial nucleus of the hypothalamus and the infundibular (arcuate) nucleus, brain nuclei that play key roles in the regulation of food intake and energy homeostasis. The posterior hypothalamic area, a target for deep brain stimulation in the treatment of cluster headaches, was readily identified, as was the lateral hypothalamic area, which similar to the aforementioned hypothalamic nuclei, could be a putative target for deep brain stimulation in the treatment of obesity. Finally, each of the identified structures was mapped to Montreal Neurological Institute (MNI) space.

Key word : MRI, human hypothalamus, anatomy, coronal plane

Introduction

Functional stereotactic neurosurgery of the hypothalamus is currently used for the treatment of cluster headaches (Leone et al., 2001; Fontaine et al., 2010; Franzini et al., 2010), and has recently been shown to have beneficial effects in the treatment of paroxysmal ophthalmic pain in multiple sclerosis patients (Cordella et al., 2009). Excitingly, it has also been shown to activate neural activity in cognitive and memory circuits in patients with mild Alzheimer's disease (Laxton et al.). Additional applications of hypothalamic deep brain stimulation may be expected in the field of sleep disorders (Vetrugno et al., 2007), thermoregulation (Jurgens et al., 2009), epilepsy (Franzini et al., 2008), disruptive behavior (Franzini et al., 2005) and perhaps certain other diseases involving the autonomic nervous system (Cortelli et al., 2007). Importantly, deep brain stimulation is also currently being investigated as a weigh loss strategy in obesity (Sani et al., 2007; Halpern et al., 2008; Hamani et al., 2008; Mantione et al.). Anatomical knowledge of the hypothalamic structures to be targeted and of the circuitry involved is thus critical to the development of these new neurosurgical treatment strategies.

The hypothalamus is the part of the diencephalon located below the thalamus; it lies along the walls of the third ventricle below the hypothalamic sulcus and continues across the floor of the ventricle (Carpenter, 1985). Despite its small size (4 g), no other brain structure contains so many specialized cell groups (Saper, 1990). The hypothalamus controls vital bodily processes including cardiovascular regulation, sleep, metabolism, stress, thermoregulation, water and electrolyte balance, appetite regulation, sexual behavior and endocrine and immune responses. All these functions are related to affective and emotional behavior. The wide range of tasks controlled by a very small part of the brain makes the hypothalamic region particularly prone to involvement in several disorders. Significantly, the human hypothalamus has been implicated in homeostatic and developmental disorders, including sudden infant death syndrome, Prader-Willi syndrome, disturbance of biological rhythms, infertility, and diabetes and obesity (Swaab, 2006; Gordon, 2010; Kalsbeek et al., 2010), as well as in episodic brain disorders such as migraine, depression, narcolepsy and cluster headaches (Overeem et al., 2002; Swaab, 2006). Besides these, the hypothalamus is

subject to many different types of lesions, including developmental abnormalities (Rathke's cleft cysts, hamartoma), primary tumors of the central nervous system (hypothalamic glioma), systemic tumors affecting the brain, inflammatory and granulomatous diseases (sarcoidosis) and lesions arising from the surrounding structures (Loes et al., 1991; Saleem et al., 2007). Notably, modern neuroimaging techniques have revealed the presence of lesions and tumors causing structural abnormalities in the hypothalamus of patients with eating disorders (Shinoda et al., 1993; De Vile et al., 1995), and the precocious onset of puberty (Jung et al., 2005; Trivin et al., 2006).

Magnetic resonance imaging is the technique of choice for evaluating the anatomy of the hypothalamus *in vivo*. However, the very small size of this region requires the use of specific high-resolution MRI sequences. The identification of gray or white matter within the hypothalamus, where some nuclei are about one millimeter across, is difficult and must be treated with caution, with frequent reference to sequential anatomical and histological sections. An atlas of the anatomical, histological and radiological correlates of the human hypothalamus in the coronal plane would thus be very useful for MRI identification of the hypothalamic structures. However, to our knowledge, such an atlas does not exist. Braak and Braak (Braak and Braak, 1987, 1992) proposed a review of the anatomy of the chiasmatic and tuberal region, but their article was only illustrated by histological staining among different species. Young and Stanton (Young and Stanton, 1994) proposed a three-dimensional reconstruction of the human hypothalamus, but this work did not contain imaging correlates. In the latest edition of their atlas of the human brain, Mai and colleagues (Mai et al., 2008) presented a macroscopic correlation between anatomical and MRI sections without the resolution necessary to identify hypothalamic nuclei in the latter. Finally, Miller and colleagues (Miller et al., 1994) examined the correlation between anatomical and MRI sections of the hypothalamus, but this was only done in vitro, while Saeki and colleagues (Saeki et al., 2001) focused their work exclusively on the white matter fascicles of the human hypothalamus.

Here, we provide a comprehensive atlas comparing anatomical, histological and magnetic resonance images of the human hypothalamus, and show that MRI, using specific sequences of acquisition, enables the clear-cut identification of several hypothalamic areas, nuclei and white matter fascicles.

Materials and methods

Population

The study was carried out with the approval of the local ethical committee and informed consent was obtained from each subject. Twenty healthy volunteers (10 men and 10 women) with a normal clinical and neurological examination and subjected to a 1.5 T MRI were used in the present study. There was no difference between the age of men (21.7 +/- 1.9 years) and women (21.3 +/- 1 years) using a Student's test for independent samples ($p > 0.05$). The Body Mass Index (BMI) was not different between the 2 groups (men: 22.7 +/- 2.7; women: 20.9 +/- 1.5 ; $p > 0.05$; Student's test).

Conventional MRI

MRI was performed on a 1.5T scanner (ACHIEVA R1.5.1, Philips, Best, The Netherlands) using a 8-channel SENSE head coil. Sequences were designed to cover the entire thalamus and hypothalamus. The anatomical limits used were the genu of the corpus callosum anteriorly, and the posterior aspect of the callosal splenium, posteriorly. The protocol included T1-weighted 3D Fast Field Echo (T13D) (TR/TE: 25/4.6 ms; NEX: 2; flip angle: 30; FOV: 230/183/60; matrix: 272x216 mm; 75 slices; voxel size: 0.85/0.85/0.80 mm), T1-weighted inversion-recovery (T1IR) (TR/TI/TE: 7910/400/15 ms; NEX: 2; FOV: 230/195/73; matrix: 512x261 mm; 20 slices; slice thickness: 3 mm; slice gap: 0.7 mm), T2-weighted Turbo Spin Echo (T2TSE) (TR/TE: 3500/100 ms; NEX: 4; flip angle: 90; TSE factor: 25; FOV: 260/183/80; matrix: 512x262 mm; 32 contiguous slices; slice thickness: 2.5 mm), T2-

weighted 2D Fast Field Echo (T2FFE) (TR/TE: 646/23 ms; NEX: 2; flip angle: 18; FOV: 250/188/73; matrix: 304x171 mm; 20 slices; slice thickness: 3 mm), all in the coronal plane.

Anatomical and histological coronal sections

For the anatomical sections, a human brain was frozen at -10 ° C for one week and then cut in the coronal plane at 5 mm intervals. The brain was taken from a patient without neurological disorders, who donated his body to science in compliance with French laws on bioethics.

For the histological sections, the brains of five women were obtained from autopsies 6-48 hrs postmortem. After whole brain removal, blocks of 20 mm per side encompassing the hypothalamus were harvested with the optic chiasm as the anterior limit and the mamillary bodies as the posterior limit. Hypothalami were immersion-fixed in 4% paraformaldehyde in 0.1 M phosphate buffer, pH 7.4, for 1 week, cryoprotected in 20% buffered sucrose for 48 h, embedded in Tissue Tek (Miles, Elkhart, IN, USA) and frozen in isopentane. Coronal cryostat sections (14 μm) were mounted on chrome-alum-gelatin coated slides, air dried, and immersed in a solution of 0.3 % Sudan Black B (Sigma, St Quentin Fallavier, France) in 70 % ethanol for ten minutes or in Nissl stain for 4 minutes. Because of the likelihood of tissue distortion during the histological sectioning process, no attempt was made to fuse histological and MRI data. Histological analyses provided the anatomical landmarks that served as standards for the reliable identification of hypothalamic areas, nuclei and white matter fascicles in MRI coronal sections and volumes.

Data analysis

An anatomist and an experienced neuroradiologist reviewed all MRI sets in order to score the visibility of gray and white structures within the hypothalamus. Structures were identified visually based on our knowledge of specific landmarks obtained from anatomical-histological cross sections and with reference to previously published atlases (Swaab et al., 1993; Koutcherov et al., 2000, 2004; Koutcherov et al., 2007; Mai et al., 2008); the landmarks used,

such as the optic tract, the floor of the diencephalon, the third ventricle, and the fornix, were readily and reliably identifiable in MR scans. Each structure was given a score as follows: 1 (non-identifiable), 2 (identifiable but poorly delineated), and 3 (identifiable and well-delineated). The agreement between the two scorers for 20 brains, as assessed by Cohen's kappa coefficient was very good ($\kappa = 0.96$, $p < 0.0001$).

All MRIs were reviewed on a Mac OS computer using the software OsiriX v. 3.2.1 (www.osirix-viewer.com). The gray and white structures that were targeted are summarized in Table 1. Other abbreviations, not expanded in Table 1, are summarized in Table 2.

For each subject, all T1 3D images acquired underwent automated linear registration onto standard Montreal Neurological Institute (MNI) coordinates system by maximizing the cross-correlation between the individual image and the MNI template (Collins et al., 1994). Since the high-resolution images acquired did not encompass the entire head, which resulted in the loss of some landmarks usually used for automated linear registration such as skull, eyes and top of the neck, quality of each registration was carefully assessed visually using the MNI-Register tool. Registrations were found to be accurate for all subjects. Individual 3D-reconstructed MRI volumes were visually inspected and the coordinates of the center of each manually identified gray and white hypothalamic structure calculated using SPM8.

Statistical analysis

Differences between MRI sequences in terms of the detection of the hypothalamic nuclei were assessed using the Friedman test (a non-parametric equivalent of a one-sample repeated measures design). A *p*-value of less than 0.05 was considered significant. A Wilcoxon signed ranks test was then done to determine the best sequence for the identification of these structures.

Results

Anatomical sections were annotated using data from the literature, especially the atlas of Mai *et al.* (Mai et al., 2008) and review articles from Braak and Braak (Braak and Braak, 1987,

1992), Swaab *et al.* (Swaab et al., 1993) and Koutcherov *et al.* (Koutcherov et al., 2000, 2002; Koutcherov et al., 2007).

All data are summarized in Tables 3 (for white matter and preoptic area) and 4 (for anterior hypothalamic area, tuberal and mammillary regions). Figures 1, 3 and 5 illustrate a series of anatomical and histological sections in the coronal plane. In Figures 2, 4 and 6 are illustrated a series of MRI sections in the coronal plane of the corresponding hypothalamic regions. All MRI images used in these figures were acquired from the same subject. Figure 7 shows the display of additional hypothalamic nuclei in different volunteers. Table 5 provides the average coordinates (n = 20 volunteers) of the identified hypothalamic areas, nuclei and white matter fascicles in anatomical MNI space.

White matter

The **diagonal band** (DB) was well identifiable both in T1 3D (high signal intensity) and in T1IR sequences (low signal intensity). It forms the posterior border of the anterior perforated substance (Fig. 7A).

The **optic tract** (opt) was remarkably easily identifiable in all sequences, except, in T1IR where it was still poorly defined in some cases. Each optic tract partially encircled the hypothalamus and the rostral portions of the crus cerebri (Fig 2, 4).

The **mammillothalamic tract** (mt) is a small structure that was sometimes identified in T13D (high signal intensity) or T2TSE sequences (without a significant difference between these two sequences). It represents the dorsal component of the principal mammillary fasciculus (Fig. 5-7). It contains fibers that project from the medial mammillary nucleus to the anterior thalamic nuclei (Carpenter, 1985).

The **principal mammillary fasciculus** (pm), was most easily identifiable in T1 3D sequences (p=0,001), followed by T2 TSE and FFE. It was clearly identified in most cases under the shape of a small high-intensity structure, concave underneath and on the outside, surrounding the mammillary nucleus (Fig . 6-7).

The **fornix** (fx) is composed of arch-shaped white matter tracts connecting the hippocampus to the mammillary body (Fig 1-7). The main parts of the fornix are the two crura, the commissure, the body and the two columns (Carpenter, 1985). Each column further divides into pre- and postcommissural fornices (25 % and 75 % respectively) at the level of the anterior commissure. The precommissural fibers extend to the septal, lateral preoptic and anterior hypothalamic nuclei. The postcommissural fornix projects to the mammillary body and terminates mainly in the medial nucleus. The fornix was easily identifiable in all sequences except T1IR.

The **anterior commissure** (ac) crosses the median plane as a compact fiber bundle immediately in front of the anterior columns of the fornix (Fig. 1). It was easily identifiable in T2 and T13D sequences (Fig 2).

The **medial forebrain bundle** (mfb) is a complex group of fibers arising from the basal olfactory regions, the septal nuclei and the periamygdaloid region, which passes to and through the lateral preoptic and lateral hypothalamic regions (Carpenter, 1985). This tract is well developed in lower vertebrates, but is small in humans (Fig.1), and it was not possible to identify it in the different MRI sequences.

Preoptic area

This region constitutes the periventricular gray of the most rostral part of the third ventricle. The **medial preoptic nucleus** (MPO) (Fig. 1) is a structure composed of predominantly small cells, indented laterally by the lateral hypothalamic area (LHA) and bulging medially toward the paraventricular nucleus (Pa) (Koutcherov et al., 2007). This nucleus was only identifiable in T13D sequence as a hyposignal (Fig. 2).

The **uncinate nucleus** (Un) has been described as being a tight group of medium-sized neurons invading the lateral boundary of the anterodorsal Pa and bordered laterally by the MPO (Fig. 1C) (Braak and Braak, 1992; Koutcherov et al., 2007). However, none of the approaches used in the present study could identify this nucleus.

The **intermediate nucleus** (InM) (or sexually dimorphic nucleus/INAH-1) was revealed with Nissl staining as a compact nuclear gray formed of a homogeneous population of nerve cells (Fig 1.C-D). The nucleus shows rounded contours and is located at the level of the optic chiasm between the supraoptic and paraventricular nucleus. The intermediate nucleus is known to be twice as large (0.20 mm^3) and contains twice as many cells in men as in women (Swaab et al., 1993). Because of its small size, this nucleus was not seen using MRI either in male or in female volunteers.

Anterior hypothalamic area

This region, also called the chiasmatic region, contains two of the most striking and sharply defined hypothalamic nuclei, the paraventricular nucleus and the supraoptic nucleus (fig. 1).

The **paraventricular nucleus of the hypothalamus** (Pa) forms a vertical plate of densely packed cells immediately beneath the ependyma of the third ventricle (Fig. 1, 3) (Carpenter, 1985; Koutcherov et al., 2000). Ventral to the fornix, the main body of the Pa rises vertically along the wall of the third ventricle throughout the preoptic and tuberal regions of the hypothalamus (Koutcherov et al., 2000). The paraventricular nucleus was seen very clearly in T1IR and in T13D sequences (Fig.2). It was also visible in T2 sequences, but not as sharply.

The **supraoptic nucleus** (SO) caps the optic chiasm and straddles the optic tract laterally (Mai et al., 1991). This nucleus is composed mainly of uniformly large cells (Fig 1). The supraoptic nucleus was usually correctly identifiable using T13D; it was not visible in other sequences (Fig 2).

The **suprachiasmatic nucleus** (SCh) is small and situated above the optic chiasm, close to the ependymal lining of the third ventricle (Fig 1). Anterolaterally, it blends into the chiasmatic gray, and posteriorly it gradually merges with the retrochiasmatic nucleus. It receives projections from the retina and is involved in the circadian rhythm (Swaab et al., 1993). It is sexually dimorphic - it is more elongated in women and more spherical in men (Swaab et al.,

1993). It was occasionally possible to pinpoint the suprachiasmatic nucleus in T13D sequences, even though its boundaries remained poorly delineated.

The **retrochiasmatic nucleus** (RC), also called the anterior hypothalamic nucleus, is localized above, between and below the fibers of the supraoptic commissures (Fig. 7B). Laterally and inferiorly it borders upon the infundibular (arcuate) nucleus of the tuberal region. It corresponds to the less well-differentiated gray of the anterior hypothalamic region. In the coronal plane, it was in isosignal but not easily identifiable, and was never seen in T1IR.

The **lateral hypothalamic area** (LHA) is bounded medially by the mammillothalamic tract and the anterior column of the fornix (Fig 1, 3, 5); its lateral boundary is the medial margin of the internal capsule and the subthalamic region. LHA could be identified using T13D MRI sequences (Fig 2, 7).

Tuberal region

In this region, the hypothalamus reaches its widest extent. Medially, it is generally possible to distinguish a ventromedial and a posteromedial nucleus. The **ventromedial nucleus of the hypothalamus** (VMH) is the largest cell group in the tuberal region. It has a round or oval shape and is surrounded by a cell-poor zone that can helps to delineate its boundaries. In the coronal plane it creates a small bulge between the median eminence and the optic tract (Fig 3C), which made identification relatively easy by MRI, particularly in T13D (Fig. 4).

The **dorsomedial hypothalamic nucleus** (DMH) is a less distinct aggregation of cells that borders the third ventricle. Indeed, the DMH is composed of a poorly differentiated group of loosely dispersed neurons whose morphology resembles the morphology of neurons of the surrounding hypothalamic gray (Braak and Braak, 1992; Koutcherov et al., 2004). The DMH covers the anterior and superior poles of the ventromedial nucleus of the hypothalamus. Its identification by MRI was difficult and, again, the T13D sequence was the most useful in highlighting it (Fig. 4, 7).

The horseshoe-shaped **infundibular nucleus** (inf) (or **arcuate nucleus of the hypothalamus**) is located in the most ventral part of the third ventricle near the entrance to the infundibular recess and extends into the median eminence (ME) (Koutcherov et al., 2002) (Fig. 3). The small cells of this nucleus are in close contact with the ependyma lining the ventricle. This nucleus was clearly visible in T13D (hypersignal) or T1IR (hyposignal) sequences (Fig. 4). T2 sequences were less useful in highlighting it.

Finally, the **perifornical nucleus** (PeF) was not identified in MRI, although it was easily identifiable by Nissl staining in the basal and lateral part of the column of the fornix (Fig 3).

Mammillary region

This region consists of the mammillary bodies and the dorsally located posterior hypothalamic nucleus (fig. 4). Each mammillary body is composed almost entirely of the large spherical **medial mammillary nucleus** (MM), consisting of relatively small cells invested by a capsule of myelinated fibers. The medial part of this nucleus was clearly visible in MRI, especially in T2TSE, T1IR and T13D sequences (Fig 5), without a significant difference between these sequences (Table 4). The lateral part of the mammillary body, the **lateral mammillary nucleus** (LM), a well-defined group of large cells (Fig 5C), were not distinctly visible in MRI.

The **lateral tuberal nucleus** (LTu) could never be identified in MRI. Between the LTu and the MM, and surrounding them, are found neurons of the **tuberomammillary nucleus** (TM), part of which accompanies the fornix (forming the perifornical nucleus). This nucleus was sometimes visible as a hyposignal in T13D sequences.

The **posterior hypothalamic area** (PH) lies dorsal to the mammillary body (Fig. 5) and caudal portions of the ventromedial nucleus of the hypothalamus. The large cells of the posterior hypothalamus are especially numerous in humans and extend caudally into the periaqueductal gray. The posterior hypothalamic area, limited on the outside by the mammillothalamic tract (mt), was fairly visible as hyposignal in T13D thanks to the identification of the mammillothalamic tract. Similarly, the **posterior part of the lateral**

hypothalamic area was identifiable by MRI because it was limited on the inside by the mammillary body and the mammillothalamic tract (fig. 3).

Discussion

This study was designed to provide an anatomical basis for the development of new treatment strategies involving functional neurosurgery by mapping gray and white structures in the living human hypothalamus. Indeed, the hypothalamus serves as a crucial centre for the integration and coordination of various brain functions, and as such, it is prone to involvement in several major brain disorders (Saper, 1990; Overeem et al., 2002; Sisk and Foster, 2004; Swaab, 2006; Aziz et al., 2007; Bao et al., 2008; Willis, 2008; Gordon, 2010; Kalsbeek et al., 2010). Precise MRI identification of the gray and white structures of the hypothalamus would also be of great help in developing new research approaches aimed at investigating hypothalamic connectivity (Lemaire *et al.*, 2011) and the functional and/or metabolic changes that occur naturally within the hypothalamus with fluctuating physiological conditions (Baroncini et al., 2010) and/or upon changes to the external environment (Goldstein et al., 2010), as well as in routine clinical examination using 1.5T MRI. Besides, detailed knowledge of hypothalamic topography *in vivo* is a prerequisite for the future development of automatic algorithms (Wang et al., 2011) that enable the accurate segmentation of the hypothalamus and its subregions (Goldstein et al., 2007), and thus the performance of morphometric MRI studies on an automated scale.

Our results are based on anatomically and histologically processed sections of the human diencephalon and hypothalamus, respectively, and their comparison with magnetic resonance images in living volunteers. The Sudan Black B served as the initial basis for the identification of fiber tracts. MRI was then used to identify them with high spatial resolution. The reproducibility of our results in many cases and comparison with existing data in humans (Carpenter, 1985; Mai et al., 2008) allowed us to identify the bulk of the fiber tracts with reasonable confidence. Furthermore the use of Nissl staining provided supplemental criteria

for the confirmation of anatomical limits and discrimination between the different tracts in addition to enabling the identification of gray structures, some of which were reliably identified by MRI, in conjunction with previously published neuroanatomical studies (Swaab et al., 1993; Koutcherov et al., 2000, 2004; Koutcherov et al., 2007; Mai et al., 2008).

Our qualitative analyses convincingly show that specific hypothalamic nuclei, areas and white matter tracts can be consistently identified using specific 1.5T MRI. To enable the identification of intra-hypothalamic structures, a compromise between the thickness of the sections and the signal-to-noise ratio had to be found. High-resolution images were thus acquired from very thin sections using weighted T13D, T1IR, T2TSE and T2FFE sequences that did not encompass the entire head, in order to keep acquisition time within reasonable limits for subjects. However, the MRI volumes acquired still retained key anatomical landmarks necessary for reliable automated linear registration onto the standard MNI coordinates system (Collins et al., 1994) enabling a probabilistic distribution of hypothalamic subregions. Interestingly, MNI coordinates can easily be transposed to Talairach space (Talairach and Tournoux, 1988) by using the appropriate transformations (Laird et al., 2010).

The present study shows that the use of specific 1.5T MRI sequences with an acquisition time compatible with routine examination approaches the resolution obtained from anatomical/histological sections. The use of such high-resolution MRI sequences noticeably facilitates the accurate identification of white matter bundles within the hypothalamus, which are subject to structural alteration in some disorders, and which are also key landmarks used in the planning of surgical approaches and electrode placement in patients. The **fornix**, which is composed of arch-shaped white matter fibers connecting the hippocampus to the mammillary body (Carpenter, 1985; Mark et al., 1993), has been suggested to play an important role in memory function (Tsivilis et al., 2008; Laxton et al., 2010) and has been shown to be morphologically altered in patients with temporal epilepsy (Supprian and Hofmann, 1997; Freeman et al., 2004; Concha et al., 2010). Its detailed examination is required for the surgical planning of transcallosal or transventricular tumor resection (Winkler et al., 1999). Within the mammillary region, the fornix that runs in between the medial

hypothalamus, where the posterior hypothalamic area resides, and the lateral hypothalamic area, a candidate target area for deep brain stimulation to trigger weight loss, constitutes, together with the **mammillo-thalamic tract** a useful anatomical landmark for the placement of deep brain stimulation electrodes for chronic cluster headaches and in putative treatments for obesity, respectively. The **anterior commissure**, along with the posterior commissure, is a classic marker used to determine the bi-commissural line, an essential landmark for the calculation of stereotaxic coordinates. The **diagonal band** consists of various fiber bundles in association with scattered large cells, which provide direct cholinergic projections to the amygdala, hippocampus and cortical mantle (Hedreen et al., 1984; Zaborszky et al., 2008). Intriguingly, postmortem analysis has demonstrated anatomical abnormalities in the vertical limb of the diagonal band of Broca in autistic patients (Kemper and Bauman, 1998). The size and the number of magnocellular neurons have been shown to vary during the course of the disease. Recent MRI studies have shown that changes in the volume of the diagonal band of Broca are associated with a global decline in cognitive status in patients at high risk of developing Alzheimer's disease (Grothe et al., 2010).

The current work also shows that some hypothalamic gray structures can be identified using 1.5T MRI with specific high-resolution sequences. The ventromedial nucleus of the hypothalamus and the infundibular (arcuate) nucleus are readily and consistently identifiable using T13D sequences, whereas T1IR and T2TSE are optimal sequences in which to spot the paraventricular nucleus of the hypothalamus and the mammillary body, respectively. The **mammillary bodies** have repeatedly been implicated in amnesia although their importance has been questioned (see for review (Vann and Aggleton, 2004)). Damage to mammillary body efferents is characteristic of thalamic strokes that cause amnesia, and mammillary body atrophy is always found in Korsakoff's amnesic syndrome, even though this atrophy may not always be the best predictor of amnesia. Although more restricted, mammillary body damage, for example, by tumors, has also been associated with amnesia (Kapur et al., 1996; Tsivilis et al., 2008), the deficits can be mild and transient (Hildebrandt et al., 2001). MRI-based anatomical studies have shown that the volume of the region containing the

mammillary bodies is increased in schizophrenic patients and non-psychotic first-degree relatives, and that this enlargement is associated with anxiety (Goldstein et al., 2007). Deep brain stimulation of the mammillary bodies and the mammillothalamic tract are currently being investigated as potential treatments for seizure control (van Rijckevorsel et al., 2005; Khan et al., 2009). The **paraventricular nucleus of the hypothalamus** is a complex motor relay, integrating essential endocrine and autonomic responses that sustain homeostasis (Thompson and Swanson, 2003; Watts et al., 2007). Neuroanatomical studies have reported alterations in the cytoarchitecture of this nucleus in patients with homeostatic control deficits, such as Prader-Willi syndrome, diabetes insipidus, depression and AIDS (Swaab et al., 1993; Swaab, 1995; Overeem et al., 2002; Swaab, 2006). Lesions in the region of the paraventricular nucleus are associated with hyperactivity of the autonomic nervous system and with diabetes insipidus (Carmel, 1980; Ropper, 1993). As for the mammillary bodies, MRI studies show that the volume of the paraventricular nucleus of the hypothalamus is abnormally enlarged in schizophrenia, which is associated with high rates of endocrine disorders (Goldstein et al., 2007). The **ventromedial nucleus of the hypothalamus** is consistently associated with the regulation of sexual behavior, appetite and metabolism, and had been implicated in the etiology of obesity (McClellan et al., 2006; Blaustein, 2008; Mietus-Snyder and Lustig, 2008). Like its near neighbor, the **infundibular nucleus** (also termed the arcuate nucleus of the hypothalamus), damage to the ventromedial nucleus of the hypothalamus has been linked to obesity syndromes in humans (Bray and Gallagher, 1975; Carmel, 1980; Lustig, 2002; Swaab, 2006). The infundibular nucleus plays a key role in relaying peripheral information to the metabolic and the reproductive brain (Dudas and Merchenthaler, 2006; Morton et al., 2006; Hill et al., 2008; Simpson et al., 2009). The ventromedial hypothalamus, which comprises both the ventromedial nucleus of the hypothalamus and the infundibular nucleus, might be an interesting site to target for body weight control in morbidly obese patients (Halpern et al., 2008). Another interesting candidate for deep brain stimulation in the treatment of obesity is the **lateral hypothalamic area**, which is a diffuse structure that can be seen using high-resolution T13D MRI

sequences and that has long been implicated in the control of feeding behavior and energy expenditure (Sawchenko, 1998). Interestingly, the stereotactic electrocoagulation of this hypothalamic area in obese patients has been shown to cause significant, although transient, appetite suppression and a slight reduction in weight (Quaade et al., 1974). In contrast, bilateral lesions have been associated with anorexia and emaciation (Carmel, 1980). Finally, the **dorsomedial hypothalamic nucleus**, which may constitute an important neural relay in the central regulation of homeostasis in humans (Dai et al., 1998; Elias et al., 2001; Koutcherov et al., 2004), as it is known to be in rodents (Bellinger and Bernardis, 2002; Thompson and Swanson, 2003), can also be spotted using the T13D MRI sequences. The target for deep brain stimulation in the treatment of chronic cluster headaches, i.e., the **posterior hypothalamic area** (Leone et al., 2001; Fontaine et al., 2010; Franzini et al., 2010), is also clearly identifiable using high-resolution T13D sequences in 1.5T MRI.

Conclusions

To our knowledge, the present study is the first to show that distinct hypothalamic gray and white structures can be readily and accurately identified and the probabilistic distribution of these hypothalamic subregions determined using 1.5T MRI with specific high-resolution sequences. By providing new insights into the anatomy of the human hypothalamus, this study should be useful both in developing new treatment strategies involving functional stereotactic surgery, as well as in the morphological inspection of the hypothalamus of patients with hypothalamus-related disorders in everyday clinical practice.

Acknowledgments

The authors wish to thank M. Demeulaere, G. Lefebvre and F. Stevendart (Laboratory of Anatomy) for their skillful help during dissections and the 20 volunteers who agreed to participate in this study.

References

Aziz NA, Swaab DF, Pijl H, Roos RA (2007) Hypothalamic dysfunction and neuroendocrine and metabolic alterations in Huntington's disease: clinical consequences and therapeutic implications. Rev Neurosci 18:223-251.
Bao AM, Meynen G, Swaab DF (2008) The stress system in depression and neurodegeneration: focus on the human hypothalamus. Brain Res Rev 57:531-553.
Baroncini M, Jissendi P, Catteau-Jonard S, Dewailly D, Pruvo JP, Francke JP, Prevot V (2010) Sex steroid hormones-related structural plasticity in the human hypothalamus. Neuroimage 50:428-433.
Bellinger LL, Bernardis LL (2002) The dorsomedial hypothalamic nucleus and its role in ingestive behavior and body weight regulation: lessons learned from lesioning studies. Physiol Behav 76:431-442.
Blaustein JD (2008) Neuroendocrine regulation of feminine sexual behavior: lessons from rodent models and thoughts about humans. Annu Rev Psychol 59:93-118.
Braak H, Braak E (1987) The hypothalamus of the human adult: chiasmatic region. Anat Embryol (Berl) 175:315-330.
Braak H, Braak E (1992) Anatomy of the human hypothalamus (chiasmatic and tuberal region). Prog Brain Res 93:3-14; discussion 14-16.
Bray GA, Gallagher TF, Jr. (1975) Manifestations of hypothalamic obesity in man: a comprehensive investigation of eight patients and a reveiw of the literature. Medicine (Baltimore) 54:301-330.
Carmel PW (1980) Surgical syndromes of the hypothalamus. Clin Neurosurg 27:133-159.
Carpenter MB (1985) Core text of Neuranatomy, 3rd Edition. Baltimore: Williams & Wilkins.
Collins DL, Neelin P, Peters TM, Evans AC (1994) Automatic 3D Intersubject Registration of MR Volumetric Data in Standardized Talairach Space. J Comput Assist Tomogr 18:192-205.
Concha L, Livy DJ, Beaulieu C, Wheatley BM, Gross DW (2010) In vivo diffusion tensor imaging and histopathology of the fimbria-fornix in temporal lobe epilepsy. J Neurosci 30:996-1002.
Cordella R, Franzini A, La Mantia L, Marras C, Erbetta A, Broggi G (2009) Hypothalamic stimulation for trigeminal neuralgia in multiple sclerosis patients: efficacy on the paroxysmal ophthalmic pain. Mult Scler 15:1322-1328.
Cortelli P, Guaraldi P, Leone M, Pierangeli G, Barletta G, Grimaldi D, Cevoli S, Bussone G, Baruzzi A, Montagna P (2007) Effect of deep brain stimulation of the posterior hypothalamic area on the cardiovascular system in chronic cluster headache patients. Eur J Neurol 14:1008-1015.
Dai J, Van Der Vliet J, Swaab DF, Buijs RM (1998) Postmortem anterograde tracing of intrahypothalamic projections of the human dorsomedial nucleus of the hypothalamus. J Comp Neurol 401:16-33.
De Vile CJ, Sufraz R, Lask BD, Stanhope R (1995) Occult intracranial tumours masquerading as early onset anorexia nervosa. Bmj 311:1359-1360.
Dudas B, Merchenthaler I (2006) Three-dimensional representation of the neurotransmitter systems of the human hypothalamus: inputs of the gonadotrophin hormone-releasing hormone neuronal system. JNeuroendocrinol 18:79-95.
Elias CF, Lee CE, Kelly JF, Ahima RS, Kuhar M, Saper CB, Elmquist JK (2001) Characterization of CART neurons in the rat and human hypothalamus. J Comp Neurol 432:1-19.
Fontaine D, Lazorthes Y, Mertens P, Blond S, Geraud G, Fabre N, Navez M, Lucas C, Dubois F, Gonfrier S, Paquis P, Lanteri-Minet M (2010) Safety and efficacy of deep brain stimulation in refractory cluster headache: a randomized placebo-controlled double-blind trial followed by a 1-year open extension. J Headache Pain 11:23-31.
Franzini A, Marras C, Ferroli P, Bugiani O, Broggi G (2005) Stimulation of the posterior hypothalamus for medically intractable impulsive and violent behavior. Stereotact Funct Neurosurg 83:63-66.

Franzini A, Messina G, Cordella R, Marras C, Broggi G (2010) Deep brain stimulation of the posteromedial hypothalamus: indications, long-term results, and neurophysiological considerations. Neurosurg Focus 29:E13.

Franzini A, Messina G, Marras C, Villani F, Cordella R, Broggi G (2008) Deep brain stimulation of two unconventional targets in refractory non-resectable epilepsy. Stereotact Funct Neurosurg 86:373-381.

Freeman JL, Coleman LT, Wellard RM, Kean MJ, Rosenfeld JV, Jackson GD, Berkovic SF, Harvey AS (2004) MR imaging and spectroscopic study of epileptogenic hypothalamic hamartomas: analysis of 72 cases. AJNR Am J Neuroradiol 25:450-462.

Goldstein JM, Jerram M, Abbs B, Whitfield-Gabrieli S, Makris N (2010) Sex differences in stress response circuitry activation dependent on female hormonal cycle. J Neurosci 30:431-438.

Goldstein JM, Seidman LJ, Makris N, Ahern T, O'Brien LM, Caviness VSJ, Kennedy DN, Faraone SV, Tsuang MT (2007) Hypothalamic abnormalities in schizophrenia: sex effects and genetic vulnerability. Biol Psychiatry 61:935-945.

Gordon CM (2010) Clinical practice. Functional hypothalamic amenorrhea. N Engl J Med 363:365-371.

Grothe M, Zaborszky L, Atienza M, Gil-Neciga E, Rodriguez-Romero R, Teipel SJ, Amunts K, Suarez-Gonzalez A, Cantero JL (2010) Reduction of basal forebrain cholinergic system parallels cognitive impairment in patients at high risk of developing Alzheimer's disease. Cereb Cortex 20:1685-1695.

Halpern CH, Wolf JA, Bale TL, Stunkard AJ, Danish SF, Grossman M, Jaggi JL, Grady MS, Baltuch GH (2008) Deep brain stimulation in the treatment of obesity. J Neurosurg 109:625-634.

Hamani C, McAndrews MP, Cohn M, Oh M, Zumsteg D, Shapiro CM, Wennberg RA, Lozano AM (2008) Memory enhancement induced by hypothalamic/fornix deep brain stimulation. Ann Neurol 63:119-123.

Hedreen JC, Struble RG, Whitehouse PJ, Price DL (1984) Topography of the magnocellular basal forebrain system in human brain. J Neuropathol Exp Neurol 43:1-21.

Hildebrandt H, Muller S, Bussmann-Mork B, Goebel S, Eilers N (2001) Are some memory deficits unique to lesions of the mammillary bodies? J Clin Exp Neuropsychol 23:490-501.

Hill JW, Elmquist JK, Elias CF (2008) Hypothalamic pathways linking energy balance and reproduction. Am J Physiol Endocrinol Metab 294:E827-832.

Jung H, Parent AS, Ojeda SR (2005) Hypothalamic hamartoma: a paradigm/model for studying the onset of puberty. Endocr Dev 8:81-93.

Jurgens TP, Leone M, Proietti-Cecchini A, Busch V, Mea E, Bussone G, May A (2009) Hypothalamic deep-brain stimulation modulates thermal sensitivity and pain thresholds in cluster headache. Pain 146:84-90.

Kalsbeek A, Fliers E, Hofman MA, Swaab DF, Buijs RM (2010) Vasopressin and the output of the hypothalamic biological clock. J Neuroendocrinol 22:362-372.

Kapur N, Thompson S, Cook P, Lang D, Brice J (1996) Anterograde but not retrograde memory loss following combined mammillary body and medial thalamic lesions. Neuropsychologia 34:1-8.

Kemper TL, Bauman M (1998) Neuropathology of infantile autism. J Neuropathol Exp Neurol 57:645-652.

Khan S, Wright I, Javed S, Sharples P, Jardine P, Carter M, Gill SS (2009) High frequency stimulation of the mamillothalamic tract for the treatment of resistant seizures associated with hypothalamic hamartoma. Epilepsia 50:1608-1611.

Koutcherov Y, Paxinos G, Mai JK (2007) Organization of the human medial preoptic nucleus. J Comp Neurol 503:392-406.

Koutcherov Y, Mai JK, Ashwell KW, Paxinos G (2000) Organization of the human paraventricular hypothalamic nucleus. J Comp Neurol 423:299-318.

Koutcherov Y, Mai JK, Ashwell KW, Paxinos G (2002) Organization of human hypothalamus in fetal development. J Comp Neurol 446:301-324.
Koutcherov Y, Mai JK, Ashwell KW, Paxinos G (2004) Organisation of the human dorsomedial hypothalamic nucleus. Neuroreport 15:107-111.
Laird AR, Robinson JL, McMillan KM, Tordesillas-Gutiérrez D, Moran ST, Gonzales SM, Ray KL, Franklin C, Glahn DC, Fox PT, Lancaster JL (2010) Comparison of the disparity between Talairach and MNI coordinates in functional neuroimaging data: validation of the Lancaster transform. Neuroimage 51:677-683.
Laxton AW, Tang-Wai DF, McAndrews MP, Zumsteg D, Wennberg R, Keren R, Wherrett J, Naglie G, Hamani C, Smith GS, Lozano AM (2010) A phase I trial of deep brain stimulation of memory circuits in Alzheimer's disease. Ann Neurol. 68:521-534
Lemaire JJ, Frew AJ, McArthur D, Gorgulho AA, Alger JR, Salomon N, Chen C, Behnke EJ, De Salles AA (2011) White matter connectivity of human hypothalamus. Brain Res, 1371:43-64.
Leone M, Franzini A, Bussone G (2001) Stereotactic stimulation of posterior hypothalamic gray matter in a patient with intractable cluster headache. N Engl J Med 345:1428-1429.
Loes DJ, Barloon TJ, Yuh WT, DeLaPaz RL, Sato Y (1991) MR anatomy and pathology of the hypothalamus. AJR Am J Roentgenol 156:579-585.
Lustig RH (2002) Hypothalamic obesity: the sixth cranial endocrinopathy. Endocrinologist 12:10-17.
Mai JK, Paxinos G, Voss T (2008) Atlas of the human brain, 3rd Edition. San Diego: Academic press.
Mai JK, Kedziora O, Teckhaus L, Sofroniew MV (1991) Evidence for subdivisions in the human suprachiasmatic nucleus. J Comp Neurol 305:508-525.
Mantione M, van de Brink W, Schuurman PR, Denys D (2010) Smoking cessation and weight loss after chronic deep brain stimulation of the nucleus accumbens: therapeutic and research implications: case report. Neurosurgery 66:E218; discussion E218.
Mark LP, Daniels DL, Naidich TP (1993) The fornix. AJNR Am J Neuroradiol 14:1355-1358.
McClellan KM, Parker KL, Tobet S (2006) Development of the ventromedial nucleus of the hypothalamus. Front Neuroendocrinol 27:193-209.
Mietus-Snyder ML, Lustig RH (2008) Childhood obesity: adrift in the "limbic triangle". Annu Rev Med 59:147-162.
Miller MJ, Mark LP, Yetkin FZ, Ho KC, Haughton VM, Estkowski L, Wong E (1994) Imaging white matter tracts and nuclei of the hypothalamus: an MR-anatomic comparative study. AJNR Am J Neuroradiol 15:117-121.
Morton GJ, Cummings DE, Baskin DG, Barsh GS, Schwartz MW (2006) Central nervous system control of food intake and body weight. Nature 443:289-295.
Overeem S, van Vliet JA, Lammers GJ, Zitman FG, Swaab DF, Ferrari MD (2002) The hypothalamus in episodic brain disorders. Lancet Neurol 1:437-444.
Quaade F, Vaernet K, Larsson S (1974) Stereotaxic stimulation and electrocoagulation of the lateral hypothalamus in obese humans. Acta Neurochir (Wien) 30:111-117.
Ropper AH (1993) Acute autonomic emergencies and autonomic storms. Boston: Little, Brown.
Saeki N, Sunami K, Kubota M, Murai H, Takanashi J, Iuchi T, Yamaura A (2001) Heavily T2-weighted MR imaging of white matter tracts in the hypothalamus: normal and pathologic demonstrations. AJNR Am J Neuroradiol 22:1468-1475.
Saleem SN, Said AH, Lee DH (2007) Lesions of the hypothalamus: MR imaging diagnostic features. Radiographics 27:1087-1108.
Sani S, Jobe K, Smith A, Kordower JH, Bakay RA (2007) Deep brain stimulation for treatment of obesity in rats. J Neurosurg 107:809-813.
Saper CB (1990) The hypothalamus. San Diego: Academic Press.
Sawchenko PE (1998) Toward a new neurobiology of energy balance, appetite, and obesity: the anatomists weigh in. J Comp Neurol 402:435-441.

Shinoda M, Tsugu A, Oda S, Masuko A, Yamaguchi T, Yamaguchi T, Tsugane R, Sato O (1993) Development of akinetic mutism and hyperphagia after left thalamic and right hypothalamic lesions. Childs Nerv Syst 9:243-245.
Simpson KA, Martin NM, Bloom SR (2009) Hypothalamic regulation of food intake and clinical therapeutic applications. Arq Bras Endocrinol Metabol 53:120-128.
Sisk CL, Foster DL (2004) The neural basis of puberty and adolescence. NatNeurosci 7:1040-1047.
Supprian T, Hofmann E (1997) The fornix of the human brain: evidence of left/right asymmetry on axial MRI scans. Surg Radiol Anat 19:105-109.
Swaab DF (1995) Development of the human hypothalamus. Neurochem Res 20:509-519.
Swaab DF (2006) The human hypothalamus in metabolic and episodic disorders. Prog Brain Res 153:3-45.
Swaab DF, Hofman MA, Lucassen PJ, Purba JS, Raadsheer FC, Van de Nes JA (1993) Functional neuroanatomy and neuropathology of the human hypothalamus. Anat Embryol (Berl) 187:317-330.
Talairach J, Tournoux P (1988) Co-planar stereotaxic atlas of the human brain Stuttgart, Germany: Georg Theime Verlag.
Thompson RH, Swanson LW (2003) Structural characterization of a hypothalamic visceromotor pattern generator network. Brain Res Brain Res Rev 41:153-202.
Trivin C, Couto-Silva AC, Sainte-Rose C, Chemaitilly W, Kalifa C, Doz F, Zerah M, Brauner R (2006) Presentation and evolution of organic central precocious puberty according to the type of CNS lesion. Clin Endocrinol (Oxf) 65:239-245.
Tsivilis D, Vann SD, Denby C, Roberts N, Mayes AR, Montaldi D, Aggleton JP (2008) A disproportionate role for the fornix and mammillary bodies in recall versus recognition memory. Nat Neurosci 11:834-842.
van Rijckevorsel K, Abu Serieh B, de Tourtchaninoff M, Raftopoulos C (2005) Deep EEG recordings of the mammillary body in epilepsy patients. Epilepsia 46:781-785.
Vann SD, Aggleton JP (2004) The mammillary bodies: two memory systems in one? Nat Rev Neurosci 5:35-44.
Vetrugno R, Pierangeli G, Leone M, Bussone G, Franzini A, Brogli G, D'Angelo R, Cortelli P, Montagna P (2007) Effect on sleep of posterior hypothalamus stimulation in cluster headache. Headache 47:1085-1090.
Wang H, Das SR, Suh JW, Altinay M, Pluta J, Craige C, Avants B, Yushkevich PA, Initiative AsDN (2011) A learning-based wrapper method to correct systematic errors in automatic image segmentation: consistently improved performance in hippocampus, cortex and brain segmentation. Neuroimage 55:968-985.
Watts AG, Salter DS, Neuner CM (2007) Neural network interactions and ingestive behavior control during anorexia. Physiol Behav 91:389-396.
Willis GL (2008) Parkinson's disease as a neuroendocrine disorder of circadian function: dopamine-melatonin imbalance and the visual system in the genesis and progression of the degenerative process. Rev Neurosci 19:245-316.
Winkler PA, Weis S, Wenger E, Herzog C, Dahl A, Reulen HJ (1999) Transcallosal approach to the third ventricle: normative morphometric data based on magnetic resonance imaging scans, with special reference to the fornix and forniceal insertion. Neurosurgery 45:309-317; discussion 317-309.
Young JK, Stanton GB (1994) A three-dimensional reconstruction of the human hypothalamus. Brain Res Bull 35:323-327.
Zaborszky L, Hoemke L, Mohlberg H, Schleicher A, Amunts K, Zilles K (2008) Stereotaxic probabilistic maps of the magnocellular cell groups in human basal forebrain. Neuroimage 42:1127-1141.

Legends :

Table 1. Gray nuclei and white matter tracts identified by MRI

Table 2. Other abbreviations, not listed in table 1.

Table 3. Results of the comparative study between the different sequences for white matter tracts and the preoptic Area. For each given white mater fascicle or the preoptic area, Friedman's test was used to determine whether there was any difference among the scores obtained with the four distinct MRI sequences. Scores were 1 for non-identifiable, 2 for identifiable but poorly delineated, and 3 for identifiable and well-delineated. MRI sequences were then ranked from the most to the least efficient: Sequence 1 > Sequence 2 > Sequence 3 > Sequence 4. A Wilcoxon signed ranks test was used to perform pairwise comparisons between MRI sequences (Sequence 1 vs. Sequence 2, Sequence 2 vs. Sequence 3 and Sequence 3 vs. Sequence 4). MRI sequences used: T1-weighted 3D Fast Field Echo (T13D), T1-weighted inversion-recovery (T1IR), T2-weighted Turbo Spin Echo (T2TSE), T2-weighted 2D Fast Field Echo (T2FFE).

Table 4. Results of the comparative study between the different sequences for the Anterior Hypothalamic Area, Tuberal and Mammillary regions. For each given nucleus or area, Friedman's test was used to determine whether there was any difference among the scores obtained with the four distinct MRI sequences. Scores were 1 for non-identifiable, 2 for identifiable but poorly delineated, and 3 for identifiable and well-delineated. MRI sequences were then ranked from the most to the least efficient: Sequence 1 > Sequence 2 > Sequence 3 > Sequence 4. A Wilcoxon signed ranks test was used to perform pairwise comparisons between MRI sequences (Sequence 1 vs. Sequence 2, Sequence 2 vs. Sequence 3 and Sequence 3 vs. Sequence 4). MRI sequences used: T1-weighted 3D Fast Field Echo

(T13D), T1-weighted inversion-recovery (T1IR), T2-weighted Turbo Spin Echo (T2TSE), T2-weighted 2D Fast Field Echo (T2FFE).

Table 5. Coordinates of the identified hypothalamic areas, nuclei and white matter fascicles in the anatomical MNI space. Coordinates acquired from 20 healthy volunteers are presented as mean ± SEM in mm.

Figure 1. Representative coronal anatomical and histological atlas sections of the anterior hypothalamic area and the preoptic region. **A,** anatomical section through the anterior commissure and the medial preoptic nucleus. **B,** Histological section colored with Sudan Black B, which highlights the anterior commissure and the optic tracts. **C,** Histological section stained with Hoechst through the medial preoptic nucleus. **D,** Magnification of the area enclosed in red in C, highlighting the MPO and the supraoptic nucleus. Scale bars = 10 mm (A), 5 mm (B & C), 2 mm (D)

Figure 2. Representative coronal 1.5T MRI atlas sections of the anterior hypothalamic area and the preoptic region. **A,** T1-weighted imaging 3D Fast Field Echo (T13D) in the coronal plane, highlighting the MPO and the SO as hyposignals. **B,** T1-weighted imaging Inversion-Recovery (T1IR) which allows the identification of the paraventricular nucleus in hyposignal as in D. **C,** T2-weighted 2D Fast Field Echo imaging (T2FFE). **D,** T2-weighted Turbo Spin Echo imaging (T2TSE). The fornix as well as the anterior commissure are displayed throughout the sequence. All MRI illustrations are derived from a single volunteer. Scale bars = 10 mm (A-D).

Figure 3. Representative coronal anatomical and histological atlas sections of the tuberal region. **A,** Anatomical section through the median eminence and the infundibular (arcuate) nucleus. **B,** Histological section stained with Sudan Black B, which highlights the fornix. **C,**

Histological section stained with Hoechst through the ventromedial hypothalamic nucleus and the infundibular (arcuate) nucleus. **D,** Magnification of the area enclosed in red in C, highlighting the fornix and the paraventricular nucleus. Scale bars = 10 mm (A), 5 mm (B & C), 2 mm (D).

Figure 4. Representative coronal 1.5T MRI atlas sections of the tuberal region. **A,** T1-weighted 3D Fast Field Echo imaging in the coronal plane, highlighting the SO and the VMH as hyposignals. **B,** T1-weighted Inversion-Recovery imaging, in which the infundibular (arcuate) nucleus can be identified in hyposignal as in D. **C,** T2-weighted 2D Fast Field Echo imaging. **D,** T2-weighted Turbo Spin Echo imaging. The fornix is visible throughout the sequence. All MRI illustrations are derived from a single volunteer. Scale bars = 10 mm (A-D).

Figure 5. Representative coronal anatomical and histological atlas sections of the mammillary region. **A,** Anatomical section through the mammillary nucleus and the posterior part of the lateral hypothalamic area. **B,** Histological section stained with Sudan Black B, which highlights the principal mammillary fasciculus. **C,** Histological section stained with Hoechst through the mammillary bodies. **D,** Magnification of the area enclosed in red in C, highlighting the dorsomedial hypothalamic nucleus. Scale bars = 10 mm (A), 5 mm (C), 2 mm (B & D).

Figure 6. Representative coronal 1.5T MRI atlas sections of the mammillary region. **A,** T1-weighted 3D Fast Field Echo imaging in the coronal plane, highlighting the medial part of the medial mammillary nucleus as an isosignal. **B,** T1-weighted Inversion-Recovery imaging. **C,** T2-weighted imaging 2D Fast Field Echo. **D,** T2-weighted imaging Turbo Spin Echo. The

fornix and mammillothalamic tract can be seen with three of the four sequences. All MRI illustrations are derived from a single volunteer. Scale bars = 10 mm (A-D).

Figure 7. Representative 1.5T MRI atlas sections identifying the diagonal bands (DB) of Broca (**A**), the retrochiasmatic nucleus (RC) (**B**), the suprachiasmatic nucleus (SCh) and the medial preoptic nucleus (MPO) (**C**), the dorsomedial nucleus of the hypothalamus (DMH), the fornix (fx) and the lateral hypothalamic area (LHA) (**C,D**), the ventromedial nucleus of the hypothalamus (VMH) (**E**), and the principal mammillary fasciculus (pm) and the mammillothalamic tract (mt) (**F**). MRI images were obtained from different volunteers. Scale bars = 10 mm.

POA	Preoptic area	Pe	Periventricular hypothalamic nucleus
		MPO	Medial preoptic nucleus
		Un	Uncinate nucleus
		InM	Intermediate nucleus (SxD)

AHA	Anterior hypothalamic area	SCh	Suprachiasmatic nucleus
		SO	Supraoptic nucleus
		Pa	Paraventricular nucleus of the hypothalamus
		LHAa	Lateral hypothalamic area (anterior part)
		RC	Retrochiasmatic nucleus (NN. Hyp ant.)

TR	Tuberal region	VMH	Ventromedial nucleus of the hypothalamus
		DMH	Dorsomedial nucleus of the hypothalamus
		PeF	Perifornical nucleus
		Inf	Infundibular nucleus (arcuate nucleus)
		LHAt	Lateral hypothalamic area (tuberal part)

MR	Mammillary region	MM	Medial mammillary nucleus, medial part
		ML	Medial mammillary nucleus, lateral part
		LM	Lateral mammillary nucleus
		Ltu	Lateral tuberal nucleus
		LHAp	Lateral hypothalamic area (posterior part)
		TM	Tuberomammillary nucleus
		PH	Posterior hypothalamus

WS	White Substance	DB	Diagonal band
		ac	Anterior commissure
		mfb	Medial forebrain bundle
		opt	Optic tract
		fx	Fornix
		pm	Principal mamillary fasciculus
		mt	Mammillo-thalamic tract

Table 1.

3V	Third ventricle
AB	Access. basal amygdaloid ncl.
AM	Anteromedial thalamic nucleus
AV	Anteroventral thalamic nucleus
bcc	Aody of corpus callosum
bfx	Aody of fornix
BST	Bed nucleus of the stria terminalis
cc	Corpus callosum
Cd	Caudate nucleus
CdM	Medial caudate nucleus
Cl	Claustrum
cp	Cerebral peduncle
ec	External capsule
EGP	External globus pallidus
Ent	Entorhinal cortex
ex	Extreme capsule
H2	Lenticular fasciculus (field H2)
HDB	Horizontal limb of the diagonal band
ic	Internat capsule
IG	Insular gyrus
IGP	Internal globus pallidus
iml	Internal medullary lamina of thalamus
infS	Infundibular stalk
La	Lateral amygdaloid nucleus
lml	Lateral medullary lamina of the globus pallidus
LSV	Ventral septal nucleus
LV	Lateral ventricle
ME	Median eminence
mml	Medial medullary lamina of the globus pallidus
ox	Optic chiasm
PaD	Paraventricular nucleus of the hypothalamus, dorsal part
PaFo	Paraventricular nucleus of the hypothalamus, fornical part
PalHy	Pallidohypothalamic nucleus
PaMc	Paraventricular nucleus of the hypothalamus, magnocellular part
PaP	Paraventricular nucleus of the hypothalamus, parvocellular part
PeF	Perifornical nucleus
Pu	Putamen
Rt	Reticular thalamic nucleus
scal	Subcallosal bundle
SODL	Supraoptic nucleus, dorsolateral part
SOVM	Supraoptic nucleus, ventromedial part
sox	Supraoptic commissure
STh	Subthalamic nucleus
TLV	Temporal horn of the lateral ventricle
VA	Ventral anterior thalamic nucleus

Table 2.

		Friedman's test	Sequence 1	p	Sequence 2	P	Sequence 3	p	Sequence 4
WS	DB	< 0.001	T1 3D	0.059	T1 IR	0.122	T2 TSE	0.033	T2 FFE
	median		2		2		2		1
	ac	< 0.001	T2 TSE	0.317	T1 3D	0.05	T2 FFE	0.285	T1 IR
	median		3		3		3		2
	mfb	-	never identified						
	opt	0.007	T1 3D	1	T2 FFE	1	T2 TSE	0.046	T1 IR
	median		3		3		3		3
	fx	< 0.001	T2 TSE	0.655	T1 3D	0.166	T2 FFE	0.01	T1 IR
	median		3		3		3		1
	pm	< 0.001	T1 3D	0.001	T2 FFE	0.527	T2 TSE	0.002	T1 IR
	median		2.5		1		1.5		1
	mt	< 0.001	T1 3D	0.058	T2 TSE	0.180	T2 FFE	0.102	T1 IR
	median		2		1		1		1
POA	MPO	<0.001	T1 3D	<0.001	T2 FFE	0.655	T1 IR	0.180	T2 TSE
	median		2		1		1		1
	Un	-	never identified						
	InM	-	never identified						

Table 3.

		Friedman's test	Sequence 1	p	Sequence 2	P	Sequence 3	p	Sequence 4
AHA	SCh	0.001	T1 3D	0.013	T1 IR	1	T2 FFE	0.046	T2 TSE
	median		1		1		1		1
	SO	<0.001	T1 3D	0.007	T2 FFE	0.132	T2 TSE	0.655	T1 IR
	median		2		1		1		1
	Pe/Pa	<0.001	T1 IR	0.003	T1 3D	0.058	T2 TSE	0.04	T2 FFE
	median		3		3		2.5		2
	LHAa	<0.001	T1 3D	<0.001	T1 IR	1	T2 FFE	0.564	T2 TSE
	median		2		1		1		1
	RC	<0.001	T1 3D	1	T2 TSE	0.705	T2 FFE	<0.001	T1 IR
	median		2		2		2		1
TR	VMH	<0.001	T1 3D	0.09	T1 IR	0.248	T2 TSE	0.083	T2 FFE
	median		3		2		2		2
	DMH	<0.001	T1 3D	<0.001	T2 FFE	0.157	T2 TSE	0.317	T1 IR
	median		2		1		1		1
	PeF	-	never identified						
	Inf		T1 3D	0.014	T1 IR	0.317	T2 FFE	0.317	T2 TSE
	median		3		3		3		2
	LHAt	<0.001	T1 3D	0.001	T2 TSE	0.059	T2 FFE	0.564	T1 IR
	median		2		1		1		1
MR	MM	0.001	T2 TSE	0.102	T1 IR	0.480	T1 3D	0.034	T2 FFE
	median		3		3		2.5		2
	ML	0.007	T2 TSE	0.492	T1 3D	.380	T2 FFE	0.046	T1 IR
	median		1		1		1		1
	LM	<0.001	T2 TSE	0.035	T2 FFE	0.083	T1 3D	1	T1 IR
	median		1		1		1		1
	Ltu	-	never identified						
	LHAp	<0.001	T1 3D	<0.001	T2 FFE	1	T2 TSE	0.046	T1 IR
	median		2		1		1		1
	TM	0.006	T1 3D	0.034	T1 IR	0.248	T2 TSE	O.655	T2 FFE
	median		2		1		1		1
	PH	<0.001	T1 3D	<0.001	T1 IR	0.317	T2 FFE	1	T2 TSE
	median		2		1		1		1

Table 4.

			MNI coordinates					
			x	SEM (x)	y	SEM (y)	z	SEM (z)
POA	Preoptic area	MPO	3.5	0.2	0.6	0.3	-13.2	0.7
AHA	Anterior hypothalamic area	SO	6.1	0.3	0.5	0.3	-15.0	0.3
		PE/Pa	2.2	0.3	-1.4	0.4	-12.3	0.4
		LHAa	6.0	0.3	-1.1	0.4	-11.9	0.3
		RC	2.9	0.3	-0.2	0.4	-18.0	0.2
TR	Tuberal region	VMH	3.6	0.4	-3.8	0.5	-16.1	0.5
		DMH	3.2	0.3	-3.0	0.2	-12.0	0.6
		Inf	2.1	0.2	-4.0	0.6	-18.1	0.2
		LHAt	6.6	0.2	-4.5	0.4	-11.4	0.5
MR	Mammillary region	MM	2.8	0.2	-8.6	0.2	-15.9	0.5
		LHAp	6.2	0.5	-9.2	0.7	-10.7	0.7
		PH	3.1	0.4	-9.1	0.6	-9.7	0.7
WS	White Substance	DB	4.5	0.2	4.1	0.8	-12.4	0.3
		ac	0.2	0.2	1.9	0.2	-4.1	0.3
		ox	0.2	0.2	4.7	0.3	-21.4	0.4
		fx [a]	4.4	0.3	-4.8	0.4	-12.2	0.4
		pm	2.5	0.3	-8.6	0.6	-12.3	0.4
		mt	4.7	0.6	-8.9	0.7	-9.1	0.2

[a] Tuberal region

Table 5.

5. Figure

Click here to download high resolution image

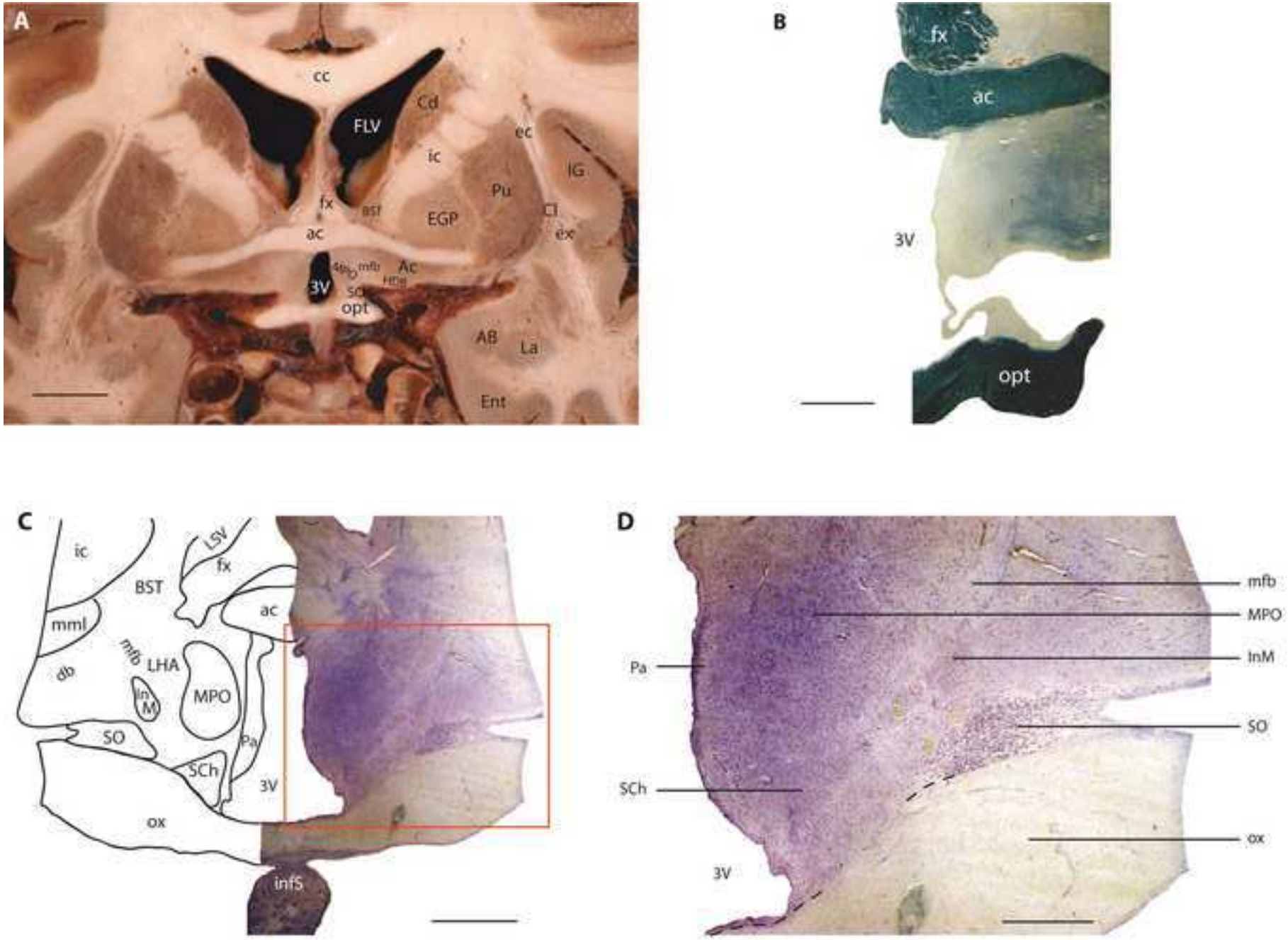

Figure 1

5. Figure

Click here to download high resolution image

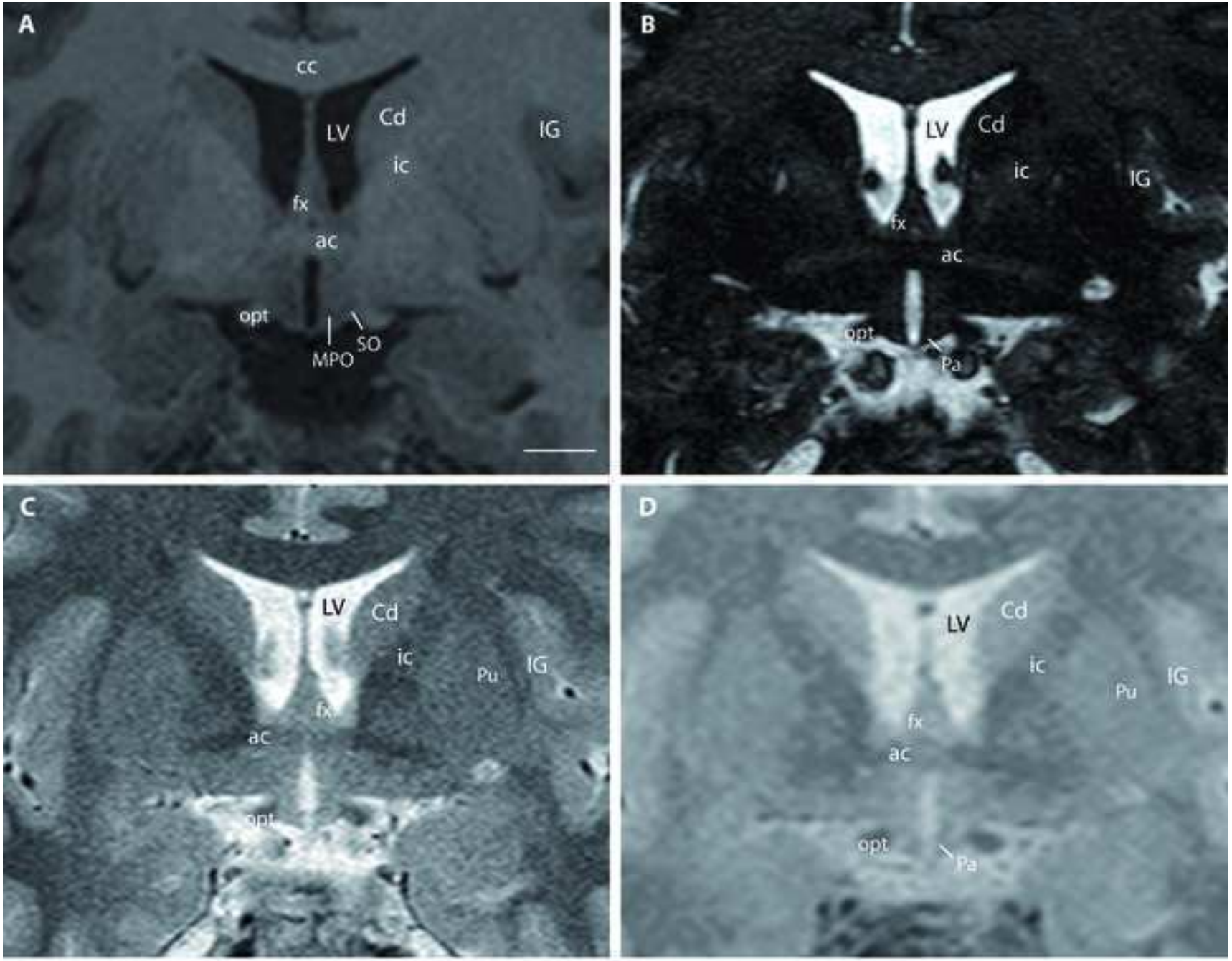

Figure 2

5. Figure

Click here to download high resolution image

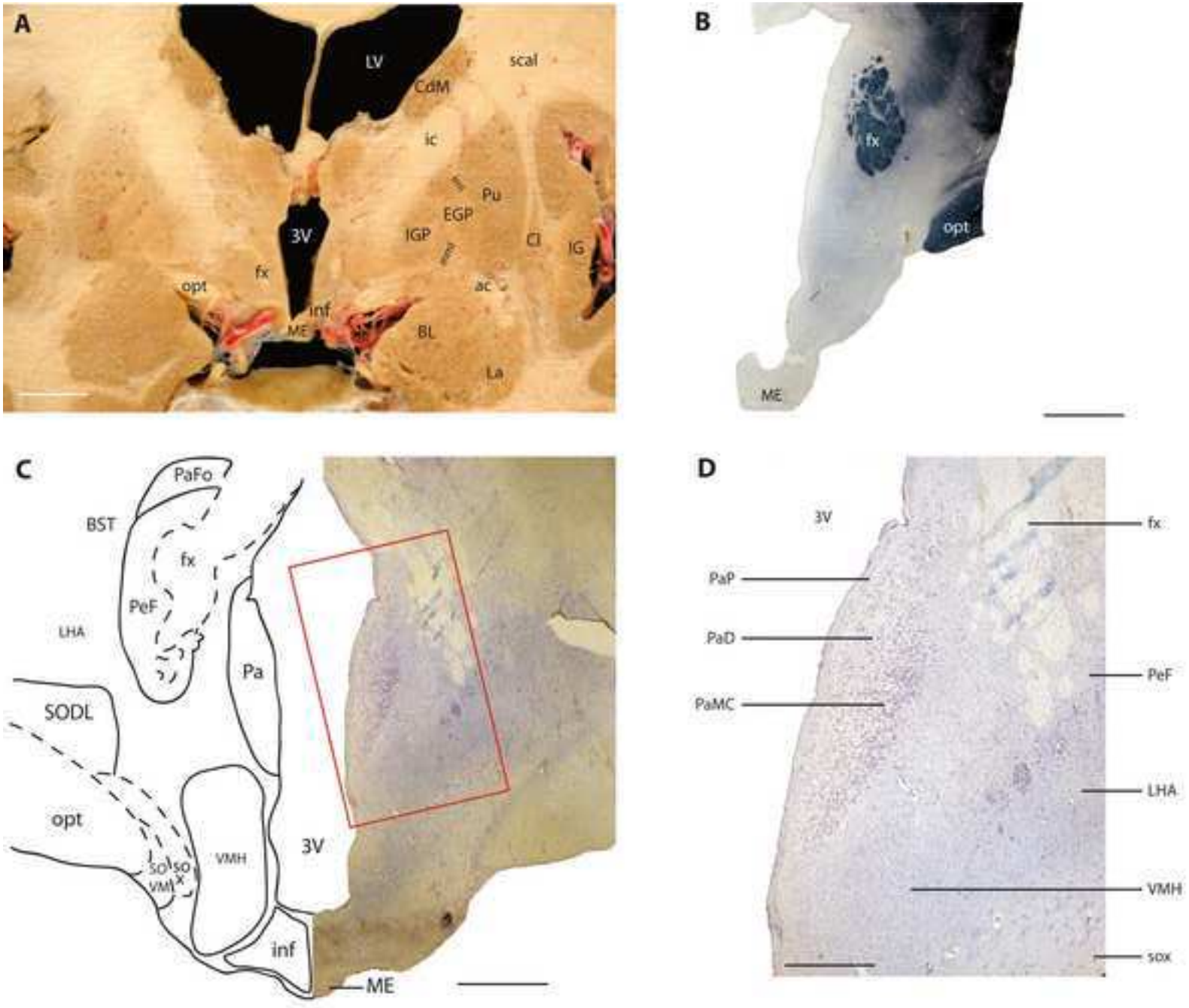

Figure 3

5. Figure

Click here to download high resolution image

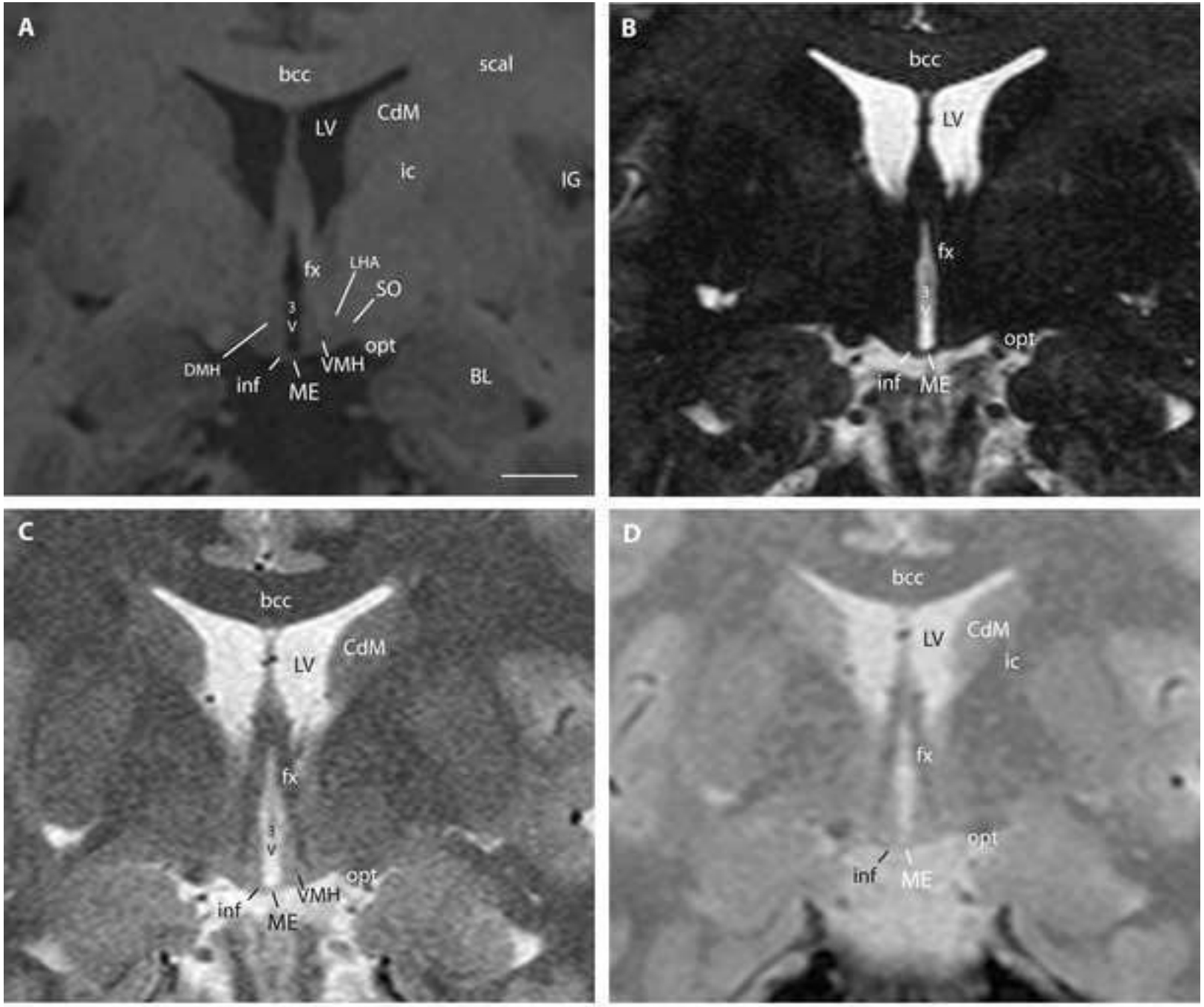

Figure 4

5. Figure

Click here to download high resolution image

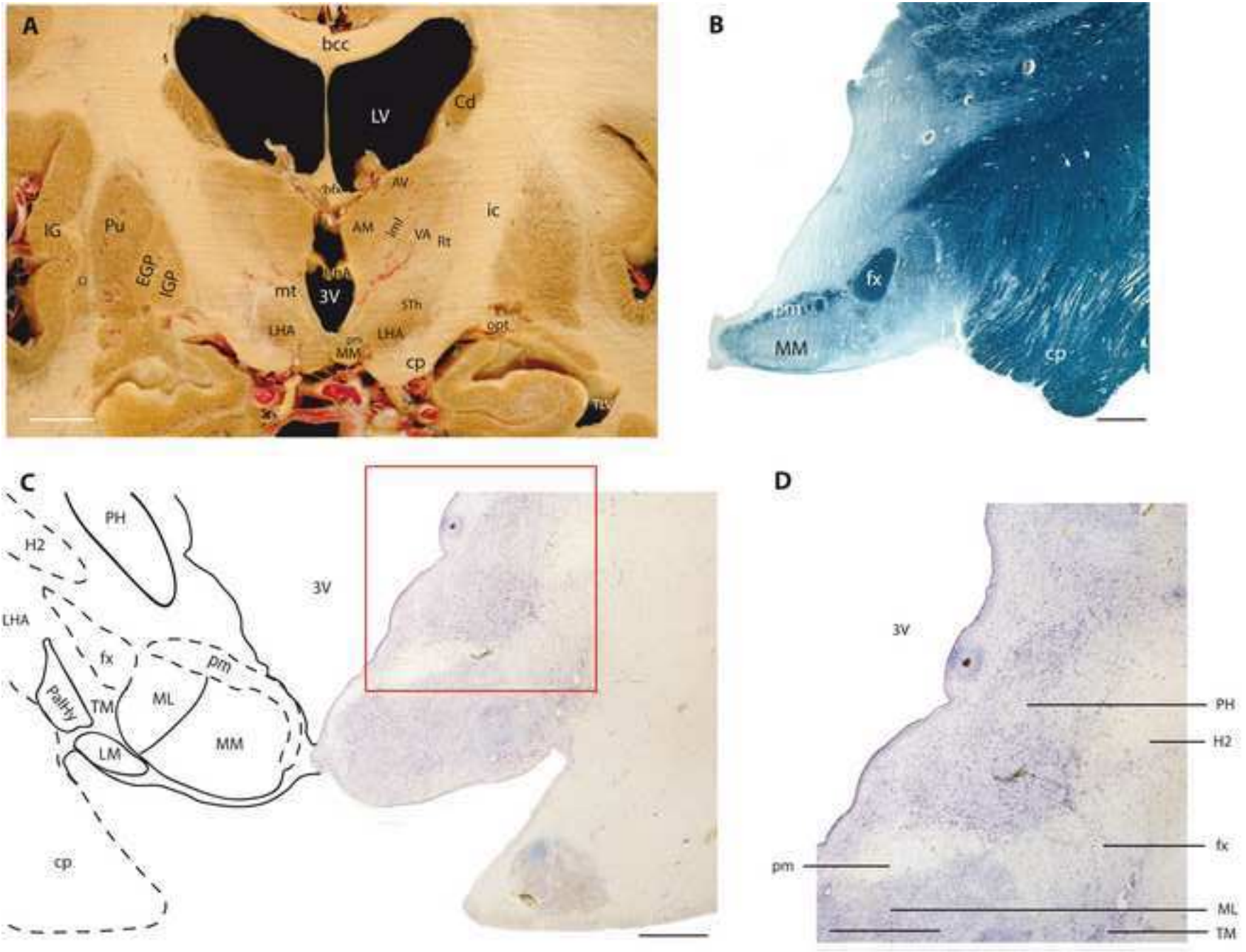

Figure 5

5. Figure

Click here to download high resolution image

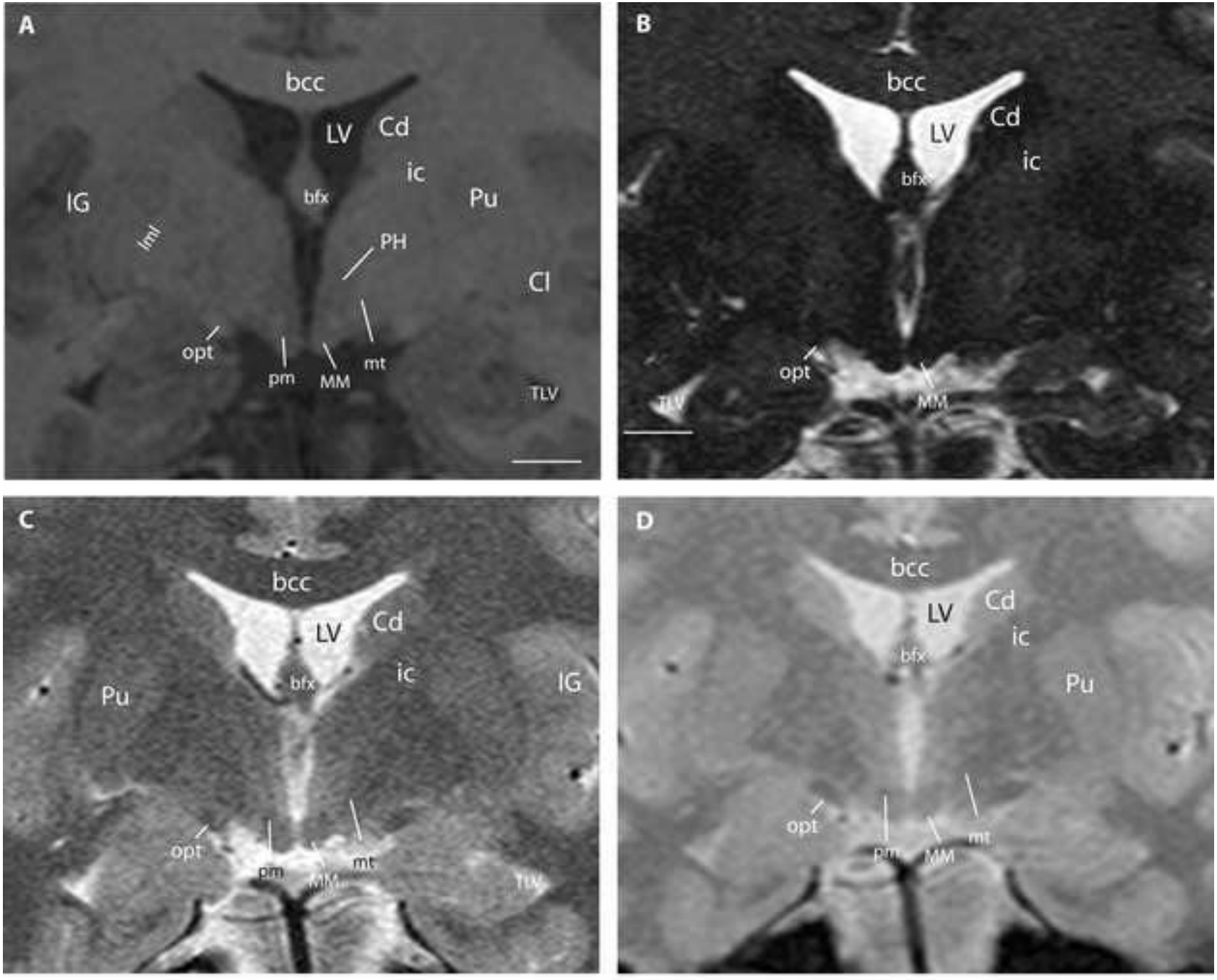

Figure 6

5. Figure
Click here to download high resolution image

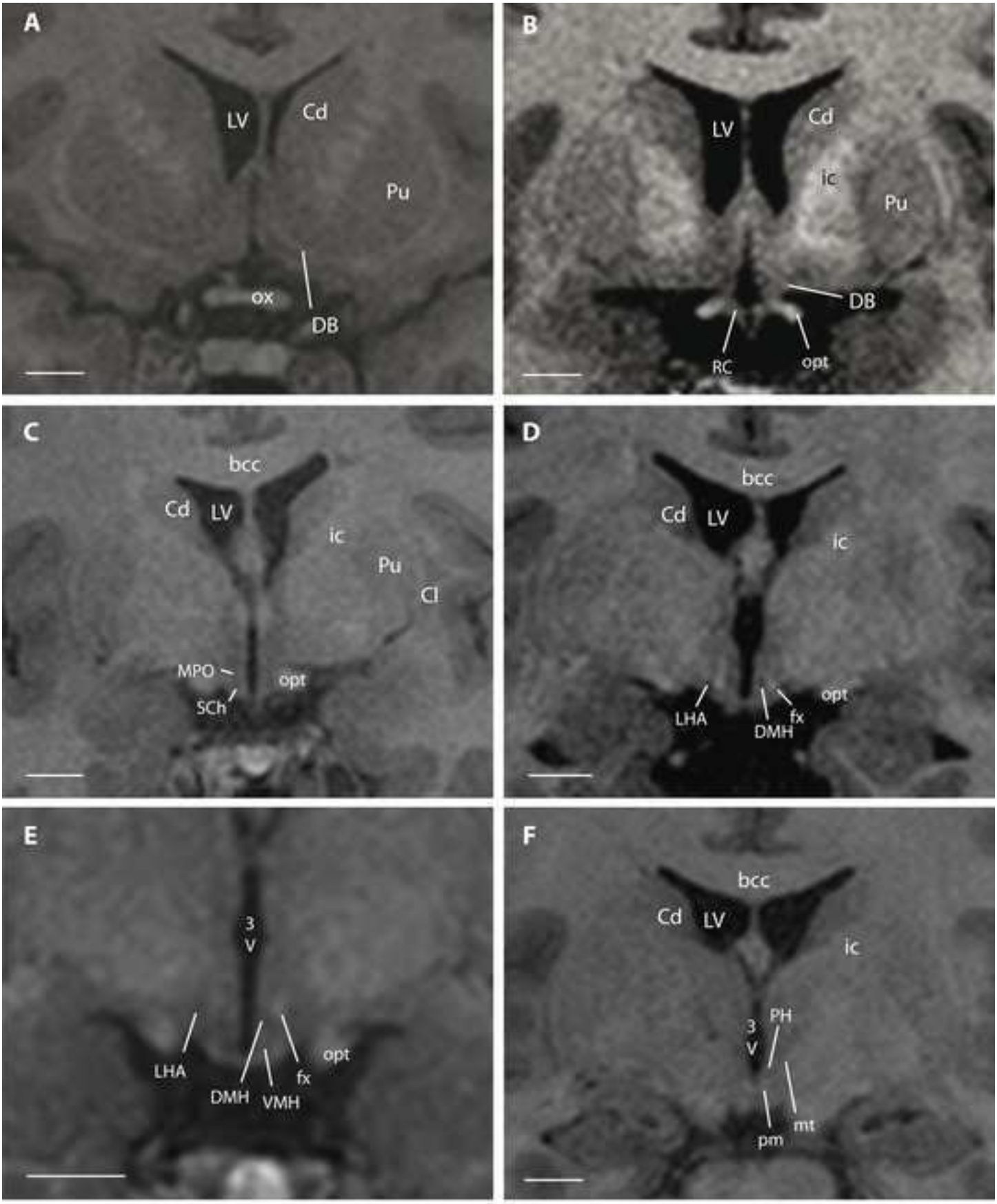

Figure 7